AIChE

Optimal Flowsheet Configuration of a Polymerization Process with Embedded Molecular Weight Distributions

Chen Zhang, Zhijiang Shao, and Xi Chen
State Key Laboratory of Industrial Control Technology, College of Control Science and Engineering, Zhejiang University, Hangzhou 310027, Zhejiang, P.R. China

Xueping Gu and Lianfang Feng
State Key Laboratory of Chemical Engineering, College of Chemical and Biological Engineering, Zhejiang University, Hangzhou 310027, Zhejiang, P.R. China

Lorenz T. Biegler
Dept. of Chemical Engineering, Carnegie Mellon University, Pittsburgh, PA 15213, USA

DOI 10.1002/aic.15040
Published online September 29, 2015 in Wiley Online Library (wileyonlinelibrary.com)

We consider the optimal reactor network synthesis of a polymerization process with detailed molecular weight distributions (MWDs). Based on an industrial high-density polyethylene (HDPE) slurry process model including an embedded MWD, a fully connected process superstructure of continuous stirred tank reactors (CSTRs) is established through the introduction of splitters. Using this generalized superstructure as a basis, two nonlinear programming (NLP) problem formulations, which simultaneously maximize the monomer conversion and minimize the deviation between the calculated and target MWDs, are developed by applying multiobjective optimization (MO) methods. Different optimal flowsheet configurations are generated by systematically manipulating a set of continuous decision variables. Several case studies that consider different specifications on MWD are conducted to illustrate the effectiveness and efficiency of the proposed synthesis approach. Numerical results show that the optimal flowsheet configurations overcome the limitations of conventional reactor network structures and help to increase reactor productivity at the desired product quality. © 2015 American Institute of Chemical Engineers *AIChE J*, 62: 131–145, 2016
Keywords: reactor network synthesis, flowsheet configuration, molecular weight distribution, multiobjective superstructure optimization

Introduction

Synthetic polymers play an essential role in everyday life. To meet extremely demanding market requirements, a polymerization process is expected to be capable of producing polymer grades with different end-use properties and rheological properties. Furthermore, increased worldwide competition, higher energy costs, and demand for lower product prices require economic efficiency from polymerization processes to a significant extent.[1] Therefore, a strong interest has motivated the determination of polymerization process configurations with wide flexibility and economic potential. Moreover, higher productivity and quality of the polymer could be achieved by optimizing reactor network structure and operating policies.[2]

Several studies[3–6] develop superstructure approaches for the reactor network synthesis problem. A general superstructure is postulated with different alternatives for the reactor network and all possible interconnections.[5] The interaction between different units of the plant can easily be represented by additional flowsheet equations.[7] On the basis of the proposed superstructure, the synthesis problem is formulated and solved to achieve a variety of objectives used for optimizing the performance of a reactor network. Achenie and Biegler[3,4] present nonlinear programming (NLP) formulations for generating optimal reactor networks based on the Jackson superstructure and the recycle reactor superstructure. They extract the optimal flowsheet configuration by systematically manipulating a set of continuous decision variables. Different test examples are considered, including the maximization of product yield and selectivity in the isothermal and nonisothermal Van de Vusse type reactions. Kokossis and Floudas[5,6] develop a superstructure for the isothermal and nonisothermal reactor systems. Their synthesis problem is addressed by formulating and solving a mixed integer nonlinear programming (MINLP) problem, which provides information on optimal reactor type and size as well as optimal operating conditions. They deal with the process designs of benzene chlorination and alkylation of benzene with ethylene to minimize the annualized plant cost and to maximize its profit.

Nevertheless, due to the complexity of the physicochemical phenomena in polymerization reactions and the nonlinearities arising from their mathematical models, reactor network

Correspondence concerning this article should be addressed to X. Chen at xichen@iipc.zju.edu.cn or L. T. Biegler at lb01@andrew.cmu.edu.

synthesis in polymerization processes remains a complicated and time-consuming task.

In polymerization processes, experimentally measured indices like melt index (MI), polydispersity index (PDI), number average molecular weight (Mn), and weight average molecular weight (Mw), are typically used to describe the polymer quality. Nevertheless, they may be insufficient to provide the complete information of the polymer. Conversely, the molecular weight distribution (MWD) is at the core in establishing key quality indices for polymers as their versatility derives from the way monomer molecules form the polymer chains.[8] Toughness, hardness, stiffness, strength, and viscoelasticity are among the properties strongly dependent upon MWD in a manner that cannot be accurately expressed by using only the above measured indices.[9] In particular, several polymer properties are closely related to the shape and breadth of the MWD. For example, high molecular weight tails and shoulders can increase the sensitivity of melt viscosity to shear rate.[10] Hence, there is a strong incentive to include detailed MWDs into models for polymer quality control and process design. A few papers focus on determining optimal operating policies of polymerization processes from target MWDs. Ali et al.[11] deal with this issue in a single reactor for the gas-phase ethylene polymerization. Their latest work[12] indicates that a predefined desired broad MWD could be achieved by proper control of the hydrogen to the monomer molar ratio inside the reactor. Pontes et al.[13] present an optimization model to determine optimal operating conditions for tailoring polyethylene with desired MWDs in a continuous ethylene polymerization process, which uses a Ziegler–Natta catalyst in a complex configuration of continuous stirred tank reactor (CSTR) and plug flow reactor (PFR). Using MWD as the designed polymer quality index, Weng et al.[14] conduct dynamic optimization on a slurry ethylene polymerization process. The optimal operating conditions are obtained through the minimization of grade transition time between two steady states.

Moreover, in the domain of polymerization process synthesis, several objectives often need to be considered simultaneously. Achieving the optimum for one objective may require some compromise for one or more other objectives.[15] For example, the requirements of high-yield production and specified polymer properties are often favored by operating policies in conflicting ways, and, thus, polymerization processes offer themselves as excellent candidates for the application of multiobjective optimization (MO).[16] MO involves several objective functions of conflicting nature,[17] which gives rise to a trade-off between all the objective functions. The goal is to obtain a set of Pareto optimal solutions, where no solution can have a better particular objective function than any other solution without compromising its other objective function values. If one moves from one Pareto solution to another, at least one objective function improves while at least one other gets worse.

Only a few studies[15–21] focus on MO for polymerization process synthesis. Asteasuain et al.[20] study a high-pressure ethylene polymerization reactor. They aim at maximizing conversion while keeping polymer polydispersity within specified values by optimizing the profiles of temperature and initiator concentration, and different reactor configurations. Later, they implement MO on a CSTR model for styrene solution polymerization.[21] The goal is to minimize the annualized reactor cost, the operating costs, the production of off-specification polymer, and the transition time between steady states. Process design includes the selection of optimal reactor size, initiator type, and steady-state operating points.

However, these studies consider only polydispersity or average molecular weights, and not MWD, as target polymer properties. Therefore, MO for polymerization process synthesis with specified MWD remains a challenging task, particularly due to the mathematical complexity of MO modeling and MWD calculation. It is expected that the optimal polymerization process design using MWD should overcome the limitations of conventional flowsheet configurations and lead to the improvement of the polymer end-use properties and productivity.

This study applies MO to the synthesis problem in polymerization processes with embedded MWDs. We first develop an equation-oriented (EO) CSTR model for a slurry-based high-density polyethylene (HDPE) polymerization process. On the basis of this HDPE slurry process, we then generalize the modeling framework to form a process superstructure consisting of CSTRs with full connectivity. The MO problem has objective functions that include maximization of monomer conversion and minimization of the deviation between the calculated and target MWDs. The optimal flowsheet configuration and operating conditions are simultaneously determined using different MO formulations. Several case studies with different specifications on MWD are then conducted to illustrate the effectiveness and efficiency of the proposed reactor network synthesis approach. The results show that the optimal structural design is a natural and intuitive choice, and straightforward to implement at industrial scale.

Model Development

HDPE is one of the most widely used synthetic commodity polymers in the manufacture of films, pipes, and containers due to the low production cost and versatility in mechanical and rheological properties. Continuous slurry polymerization with heterogeneous Ziegler–Natta catalysts is an important industrial process for HDPE production, in which polymer grows at the active sites on the catalyst until chain transfer occurs, thus, forming dead polymer chains.[22] In the slurry process, CSTRs are used to produce HDPE. The major advantages[8] of this HDPE process include mild operating conditions, excellent heat transfer capabilities, high monomer conversion rates, and relative ease of processing. Moreover, different active sites of the heterogeneous Ziegler–Natta catalysts, even on the same catalyst particle, can have different propagation rate constants, which can give rise to a very broad MWD.[22]

CSTR model

A complete EO model is established for a single CSTR system. The perturbed-chain statistical associating fluid theory equation of state (PC-SAFT EOS)[23] is used to model the thermodynamic properties. As this complex EOS model is difficult to solve by the EO approach, a set of surrogate kriging[24] models, based on the data generated from PC-SAFT EOS, was applied from our previous work.[25] Phase equilibrium, mass and energy equations were also incorporated from our previous work.[26] The kinetics and MWD models are presented next.

Homopolymerization Kinetics. The kinetic mechanism of ethylene homopolymerization with Ziegler–Natta catalyst system is summarized in Table 1, where C_P is a potential active site of catalyst $TiCl_4$, A is co-catalyst $Al(C_2H_5)_3$, M is monomer, H_2 is hydrogen, P_0 is an active site, C_d is a deactivated site, D_n is a dead polymer of chain length n, P_n is a living

Table 1. Kinetic Mechanism of Homopolymerization

Reaction Types	Descriptions
Activation	$C_p(j)+A\xrightarrow{k_{aA}(j)}P_0(j)$
Initiation	$P_0(j)+M\xrightarrow{k_i(j)}P_1(j)$
Propagation	$P_n(j)+M\xrightarrow{k_p(j)}P_{n+1}(j)$
Transfer to monomer	$P_n(j)+M\xrightarrow{k_{tM}(j)}P_1(j)+D_n(j)$
Transfer to hydrogen	$P_n(j)+H_2\xrightarrow{k_{tH}(j)}P_0(j)+D_n(j)$
Transfer to co-catalyst	$P_n(j)+A\xrightarrow{k_{tA}(j)}P_0(j)+D_n(j)$
Transfer β-hydride	$P_n(j)\xrightarrow{k_t(j)}P_0(j)+D_n(j)$
Deactivation	$P_n(j)\xrightarrow{k_d(j)}C_d(j)+D_n(j)$
	$P_0(j)\xrightarrow{k_d(j)}C_d(j)$

polymer chain of length n, j represents the index of active sites, and k_{aA}, k_i, k_p, k_{tM}, k_{tH}, k_{tA}, k_t, k_d are the kinetic rate constants of different reactions.

The Arrhenius equation is used to determine the kinetic rate constant k

$$k=k^0\exp\left[-\frac{E^a}{\overline{R}}\left(\frac{1}{T}-\frac{1}{T_{\text{ref}}}\right)\right] \tag{1}$$

where k^0 is the pre-exponential kinetic rate constant, E^a is the activation energy, $\overline{R}$ is the universal gas constant, T is the reaction temperature, and T_{ref} is the reference temperature.

Heterogeneous Ziegler–Natta catalysts possess multiple active sites, even on the same catalyst particle. The traditional approach to model the multiple sites is to assume distinct site types with different kinetic rate constants. We also assume that one type of active site cannot turn into a different type. The number of active sites is determined by the deconvolution of polymer distributions. As seen from our previous work[24] and the numerical results below, the model with five active sites fits the data well.

According to the mechanism in Table 1, we define the following pseudo-kinetic rate constant for transfer and deactivation

$$K_{\text{TD}}(j)=k_{tM}(j)[M]+k_{tH}(j)([H_2])^{0.5}+k_{tA}(j)[A]+k_t(j)+k_d(j) \tag{2}$$

where [.] denotes the concentration of the species in the reactor.

For living chains of length $n=1$, the net reaction rate takes the form

$$\begin{aligned}r_{P_1(j)}=&k_i(j)[M][P_0(j)]+k_{tM}(j)[M]Y^0(j)\\&-k_p(j)[M][P_1(j)]-K_{\text{TD}}(j)[P_1(j)]\end{aligned} \tag{3}$$

where $Y^0(j)=\sum_{n=1}^{\infty}[P_n(j)]$ is the sum of living chain concentrations.

For living chains of length $n\geq 2$, the net reaction rate takes the form

$$r_{P_n(j)}=\left(k_p(j)[M]([P_{n-1}(j)]-[P_n(j)])\right)-K_{\text{TD}}(j)[P_n(j)] \tag{4}$$

Similarly, the net reaction rate for dead chains of length $n=1$ is given by

$$r_{D_1(j)}=K_{\text{TD}}(j)[P_1(j)]-k_{tM}[M][P_1(j)] \tag{5}$$

and the net reaction rate for dead chains of length $n\geq 2$ becomes

$$r_{D_n(j)}=K_{\text{TD}}(j)[P_n(j)] \tag{6}$$

The net reaction rates for potentially active, active, and deactivated sites of catalyst can be calculated as follows

$$r_{C_p(j)}=-k_{aA}(j)[A]\left[C_p(j)\right] \tag{7}$$

$$\begin{aligned}r_{P_0(j)}=&-k_i(j)[M][P_0(j)]-k_d(j)[P_0(j)]+k_{aA}(j)[A]\left[C_p(j)\right]\\&+\left(k_{tH}(j)([H_2])^{0.5}+k_{tA}(j)[A]+k_t(j)\right)Y^0(j)\end{aligned} \tag{8}$$

$$r_{C_d(j)}=k_d(j)\left([P_0(j)]+Y^0(j)\right) \tag{9}$$

For chain lengths with $n=1, 2, 3, \ldots, n_{\max}$, the above equations can be solved to obtain the complete chain length distribution. $n_{\max}$ is the maximum chain length. However, for high MW polymers like HDPE, where $n_{\max}$ is 10^5 or more, the resulting system leads to a prohibitive number of equations and computational cost. Instead, the method of moments[27,28], calculating the leading moments of the chain length distribution with considerably less effort, is used to describe the mass balance of the polymer components. The rth moment of a generic distribution $f(x)$ is defined as

$$\mu^r=\sum_{x=1}^{\infty}x^r f(x) \tag{10}$$

so that the rth moments of living and dead polymer at the jth active site are given by

$$Y^r(j)=\sum_{n=1}^{\infty}n^r[P_n(j)] \tag{11}$$

$$X^r(j)=\sum_{n=2}^{\infty}n^r[D_n(j)] \tag{12}$$

For the zeroth moments of CLD of the living and dead polymer chains, the equations are derived by substituting the corresponding net reaction rates into the moment expressions

$$r_{Y^0(j)}=k_i(j)[M][P_0(j)]+k_{tM}(j)[M]Y^0(j)-K_{\text{TD}}(j)Y^0(j) \tag{13}$$

$$r_{X^0(j)}=K_{\text{TD}}(j)Y^0(j)-k_{tM}[M][P_1(j)] \tag{14}$$

For the first and second moments of CLD of the living and dead polymer chains, the net reaction rates are given by

$$\begin{aligned}r_{Y^1(j)}=&k_i(j)[M][P_0(j)]+k_p(j)[M]Y^0(j)\\&+k_{tM}(j)[M]Y^0(j)-K_{\text{TD}}(j)Y^1(j)\end{aligned} \tag{15}$$

$$r_{X^1(j)}=K_{\text{TD}}(j)Y^1(j)-k_{tM}[M][P_1(j)] \tag{16}$$

$$\begin{aligned}r_{Y^2(j)}=&k_i(j)[M][P_0(j)]+k_{tM}(j)[M]Y^0(j)\\&+k_p(j)[M](2Y^1(j)+Y^0(j))-K_{\text{TD}}(j)Y^2(j)\end{aligned} \tag{17}$$

$$r_{X^2(j)}=K_{\text{TD}}(j)Y^2(j)-k_{tM}[M][P_1(j)] \tag{18}$$

Typically, the zeroth, first, and the second moments are sufficient for the computation of common polymer properties like Mn, Mw, and PDI.

MWD Calculation. In the steady-state slurry process, the chain length distribution for HDPE polymerization at site j is given by a single-parameter equation, Flory's most probable distribution[29–33]

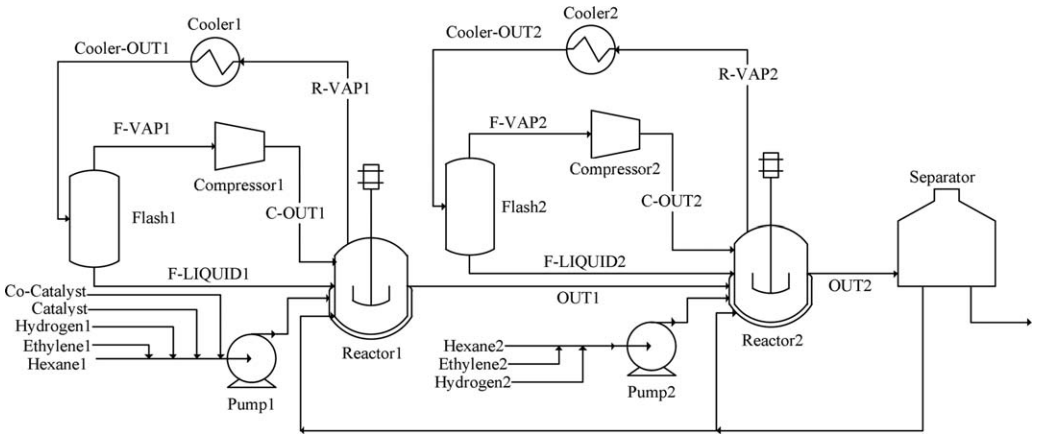

Figure 1. Flowsheet configuration of HDPE slurry process in series.

$$\tau_j = \frac{K_{\mathrm{TD}}(j)}{K_P(j)} = \frac{k_{tM}(j)[M] + k_{tH}(j)([H_2])^{0.5} + k_{tA}(j)[A] + k_t(j) + k_d(j)}{k_p(j)[M]} \tag{19}$$

$$\mathrm{cld}_j = n\tau_j^2/(1+\tau_j)^{n+1}, \quad n = 1, 2, 3, \ldots, n_{\max} \tag{20}$$

where cld_j is the weight chain length distribution of the polymer chains with length n, $n = 1, 2, 3, \ldots, n_{\max}$, τ_j is the ratio of all the chain transfer rates to the propagation rate. The following transformations[34] convert CLD to MWD on the logarithmic scale, where mw is the molecular weight of ethylene, and mwd_j is the weight distribution at the jth active site on the logarithmic scale of molecular weight

$$\mathrm{mwd}_j = \ln(10) \times (\mathrm{mw} \times n)^2 \left(\frac{\tau_j}{\mathrm{mw}}\right)^2 \left(\frac{1}{1+\tau_j}\right)^{n+1}, \quad n = 1, 2, 3, \ldots, n_{\max} \tag{21}$$

The entire distribution of the molecular weight for a single reactor, $\overline{\mathrm{mwd}}$, can be obtained using the weighted superposition of Flory's distribution from each site

$$\overline{\mathrm{mwd}} = \sum_{j=1}^{Ns} \mathrm{mwd}_j mf_j \tag{22}$$

where N_S is the number of catalyst active sites and mf_j is the mass fraction of the polymer produced at site j

$$mf_j = \frac{Y^1(j) + X^1(j)}{\sum_{k=1}^{Ns} \left(Y^1(k) + X^1(k)\right)} \tag{23}$$

The complete steady-state model of a single CSTR system, including kinetic mechanism, thermodynamics, MWD

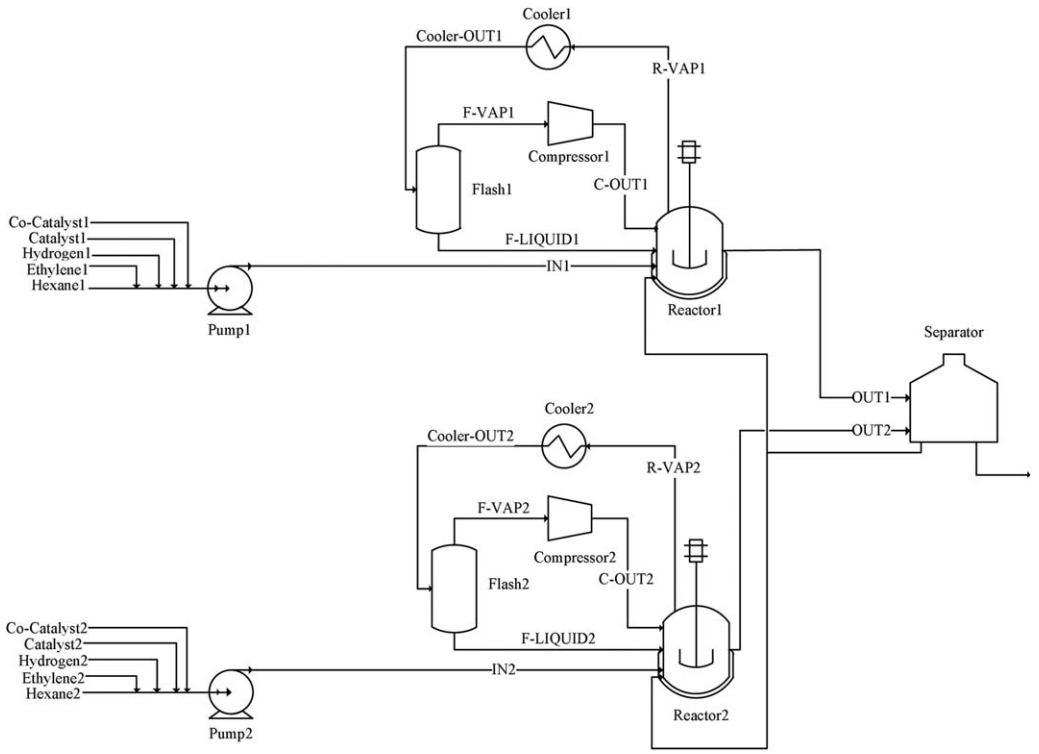

Figure 2. Flowsheet configuration of HDPE slurry process in parallel.

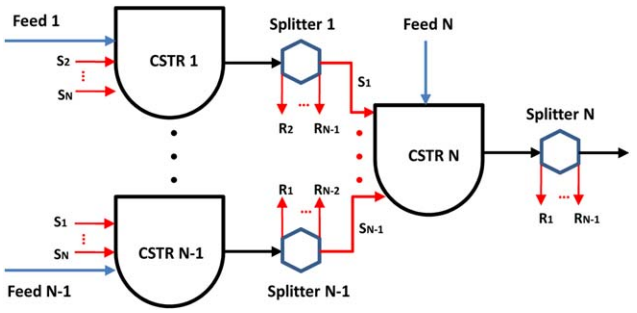

Figure 3. Superstructure of polymerization process (*N* CSTRs).

[Color figure can be viewed in the online issue, which is available at wileyonlinelibrary.com.]

calculation, phase equilibrium, and mass and energy balance, contains over 2000 variables and equations.

Flowsheet configuration

Figure 1 illustrates the flowsheet of an industrial HDPE slurry process[35] on the basis of the CX polymerization technology from Mitsui Chemicals with a Ziegler–Natta catalyst, titanium tetrachloride ($TiCl_4$), and triethyl aluminum ($Al(C_2H_5)_3$) as the co-catalyst. The current process is carried out in two isothermal CSTRs in series, together with other units including flash drums, coolers, compressors, and pumps. Ethylene (monomer), hydrogen (chain transfer agent), *n*-hexane (diluent), and the Ziegler–Natta catalyst system are fed continuously to the first CSTR. The polymer stream leaving the first reactor is fed into the second reactor together with fresh ethylene, hydrogen, and hexane. The vapor streams leaving reactors, which contain ethylene, hydrogen, and hexane, is recycled to the feed streams through coolers, flash drums, and compressors to achieve high monomer conversion. The highly concentrated slurry product leaving the second reactor is fed to a centrifugal separator that removes unreacted monomer and diluent from the polymer solids. The diluent is then completely recovered while the polymer product is dried and pelletized. Figure 2 shows the parallel configuration. It works in a very similar way as the serial configuration, except that the two CSTRs must receive identical feed streams and operate under the same conditions.[35] The polymer slurry streams leaving the two CSTRs are mixed and flow into the centrifugal separator. In our previous work,[25,26] models of these two configurations were validated using multiple plant datasets from HDPE grades produced in an industrial HDPE slurry process.

Serial and parallel flowsheet configurations in Figures 1 and 2 are frequently used in practice. However, due to the limitations of these conventional reactor network structures, many polymer grades, especially some high-quality ones, may not be available even under a wide range of operating conditions. Hence, a more flexible process flowsheet configuration needs to be considered and designed.

Superstructure model

Using the above CSTR model, we now consider the process synthesis problem associated with the reactor network superstructure. Different from conventional serial or parallel flowsheet configurations, a superstructure is constructed to incorporate all possible structural alternatives of interest. The basic idea in our work is to place splitters at the exits of CSTRs and then connect CSTRs with each other. As shown in Figure 3, we generalize the modeling framework to form a process superstructure consisting of N (≥ 2) CSTRs with full connectivity. For simplicity, the recycled vapor streams are not shown here. $N-1$ polymer substreams from each splitter are fed into other CSTRs. On the splitters, the red arrows marked by $R_1, R_2, \ldots, R_{N-1}$ represent the substreams flowing into CSTRs 1, 2, ..., $N-1$, respectively. On the CSTRs, the red arrows marked by $S_1, S_2, \ldots, S_N$ represent the substreams flowing from Splitters 1, 2, ..., N, respectively. These substreams are assumed to be well-mixed and then fed into CSTRs to participate in further reactions. Based on the slurry process technology, CSTR N is used to avoid simple mixing of HDPE grades with different MWDs from CSTRs 1, 2, ..., $N-1$. For Splitter N, there is one polymer stream flowing into downstream process units, after which a uniform polymer product is obtained.

The equations that describe the superstructure connectivity corresponding to Figure 3 are listed as follows.

1. Summation of Split Fractions

$$\sum_{m=1,m\neq l}^{N} F_{l,m}=1,\ \ l=1,\ ...,\ N-1 \tag{24}$$

$$\sum_{m=0}^{N-1} F_{N,m}=1 \tag{25}$$

where $F_{l,m}(l \neq m)$ is the stream split fraction from the exit of CSTR l to the entrance of CSTR m for Splitters 1, 2, ..., N. In particular, $F_{N,0}(>0)$ is the stream split fraction from the exit of CSTR N to downstream process units for Splitter N.

2. CSTR Mass Balance ($m=1,\ 2,\ \ldots,\ N$)

$$\begin{aligned}&(\mathrm{FEED}(M)_m+\sum_{l=1,l\neq m}^{N} F_{l,m}\mathrm{OUT}_l[M]_l)-\mathrm{OUT}_m[M]_m\\&=\sum_{j=1}^{Ns}\left(k_i(j)_m[P_0(j)]_m+\left(k_p(j)_m+k_{tM}(j)_m\right)Y^0(j)_m\right)[M]_m*V_m\end{aligned} \tag{26}$$

$$\begin{aligned}&(\mathrm{FEED}(H_2)_m+\sum_{l=1,l\neq m}^{N} F_{l,m}\mathrm{OUT}_l[H_2]_l)-\mathrm{OUT}_m[H_2]_m\\&=\sum_{j=1}^{Ns}k_{tH}(j)_m[H_2]_m^{0.5}Y^0(j)_m*V_m\end{aligned} \tag{27}$$

$$(\mathrm{FEED}(C_6H_{14})_m+\sum_{l=1,l\neq m}^{N} F_{l,m}\mathrm{OUT}_l[C_6H_{14}]_l)-\mathrm{OUT}_m[C_6H_{14}]_m=0 \tag{28}$$

$$\begin{aligned}&(\mathrm{FEED}(A)_m+\sum_{l=1,l\neq m}^{N} F_{l,m}\mathrm{OUT}_l[A]_l)-\mathrm{OUT}_m[A]_m\\&=\sum_{j=1}^{Ns}\left(k_{aA}(j)_m[C_P(j)]_m+k_{tA}(j)_mY^0(j)_m\right)[A]_m*V_m\end{aligned} \tag{29}$$

$$\begin{aligned}&(\mathrm{FEED}(C_P(j))_m+\sum_{l=1,l\neq m}^{N} F_{l,m}\mathrm{OUT}_l[C_P(j)]_l)-\mathrm{OUT}_m[C_P(j)]_m\\&=-(r_{C_p(j)})_m*V_m\end{aligned} \tag{30}$$

$$(\mathrm{FEED}(C_d(j))_m + \sum_{l=1,l\neq m}^{N} F_{l,m}\mathrm{OUT}_l[C_d(j)]_l) - \mathrm{OUT}_m[C_d(j)]_m = -(r_{C_d(j)})_m * V_m \tag{31}$$

$$(\mathrm{FEED}(P_0(j))_m + \sum_{l=1,l\neq m}^{N} F_{l,m}\mathrm{OUT}_l[P_0(j)]_l) - \mathrm{OUT}_m[P_0(j)]_m = -(r_{P_0(j)})_m * V_m \tag{32}$$

$$(\mathrm{FEED}(Y^r(j))_m + \sum_{l=1,l\neq m}^{N} F_{l,m}\mathrm{OUT}_l Y^r(j)_l) - \mathrm{OUT}_m Y^r(j)_m = -(r_{Y^r(j)})_m * V_m, \quad r=0,1,2 \tag{33}$$

$$(\mathrm{FEED}(X^r(j))_m + \sum_{l=1,l\neq m}^{N} F_{l,m}\mathrm{OUT}_l X^r(j)_l) - \mathrm{OUT}_m X^r(j)_m = -(r_{X^r(j)})_m * V_m, \quad r=0,1,2 \tag{34}$$

where the subscripts l, m denote CSTRs l and m, respectively. $FEED(.)$ denotes the flow rate of the species fed into the CSTR. OUT denotes the total flow rate out of the CSTR. V denotes the liquid volume of the CSTR.

3. CSTR MWD Calculation ($m=1, 2, \ldots, N$)

$$\mathrm{MWD}_m = \left(G_m\overline{\mathrm{mwd}}_m + \sum_{l=1,l\neq m}^{N} F_{l,m}G_l\mathrm{MWD}_l\right) \Big/ \left(G_m + \sum_{l=1,l\neq m}^{N} F_{l,m}G_l\right) \tag{35}$$

where MWD_l and $\overline{\mathrm{MWD}}_m$ are the MWDs out of CSTRs l and m, respectively. $\overline{\mathrm{mwd}}_m$ denotes the instantaneous MWD generated in CSTR m. G_l and G_m denote the polymer masses out of CSTRs l and m, respectively.

The introduction of splitters associated with CSTRs is easy to realize in practice, and the transfer of polymer substreams between any two CSTRs can be easily established by using pumps. Any particular flowsheet configuration simply becomes a special case of the general superstructure.

Typically, a superstructure contains binary variables denoting the existence of process units in addition to continuous decisions about the values for the process variables.[36] Here, we only use continuous variables, the split fraction $F_{i,j}$, to represent the existence of process units and streams. In the superstructure of N CSTRs, Splitter N does not exist when its values of $N-1$ fractions are zero. The outlet stream of CSTR N flows into another CSTR or downstream process units directly. For Splitters 1, 2, …, $N-1$, if the values of $N-2$ fractions in one splitter are zero, it means this splitter does not exist. The corresponding CSTR outlet stream flows into another CSTR directly. For all other cases, the splitter does exist. Therefore, the resulting mathematical model leads naturally to an NLP problem, which reduces problem size and complexity. As seen from the numerical results below, the structural optimization problem can be solved locally with considerably less computational effort. Moreover, a multistart procedure is used to promote the search for global solutions.

Problem Statement for Multiobjective Superstructure Optimization

Our optimization is driven by an economic criterion to maximize the reactor productivity at the desired product quality. Specifically, MO is implemented to deal with the tradeoffs arising from the simultaneous consideration of the two conflicting objectives, maximization of monomer conversion and minimization of the deviation between the calculated and target MWDs. Based on the superstructure, the optimal design of the process flowsheet configuration and operating conditions are determined using different MO formulations.

The literature abounds with MO studies for engineering systems. A comprehensive overview can be found in the book by Miettinen.[37] MO problems are often solved by scalarization, where the problem is converted into a single objective optimization problem, and well-developed methods for single objective optimization are applied to generate Pareto optimal solutions. Mathematically, the problem is solved when the feasible Pareto optimal set is obtained. Several popular methods are introduced below.[37]

1. Weighted Sum Method

In this method, each objective function is associated with a weighting factor to minimize the weighted sum of the objectives. In this way, multiple objective functions are transformed into a single real-valued objective function. The MO problem becomes

$$\begin{aligned} &\min \sum_{k=1}^{Q} w_k * f_k(x) \\ &\text{s.t. } x \in S \\ &w_k \geq 0, \quad k=1, \ldots, Q \end{aligned} \tag{36}$$

with $Q(\geq 2)$ objective functions $f_k: R^n \rightarrow R$. The decision vector $x=(x_1, x_2, \ldots, x_n)^T$ belongs to the feasible region S, which is a subset of the decision variable space R^n. w_k is the kth weighting factor. Pareto optimality is guaranteed if the weighting factors are all positive. Different Pareto optimal solutions can be generated by altering these weighting factors. The weakness of the weighted sum method is that not all of the Pareto optimal solutions can be found unless the problem is convex.

2. ε-Constraint Method

In this method, one of the objective functions is selected to be optimized and all the others are converted into constraints by setting an upper bound on each of them. The problem is given by

$$\begin{aligned} &\min f_l(x) \\ &\text{s.t. } x \in S \\ &f_j(x) \leq \varepsilon_j, \quad j=1, \ldots, Q, j \neq l \end{aligned} \tag{37}$$

where ε_j is the jth upper bound. In principle, the ε-constraint method allows all of the Pareto optimal solutions to be found by altering the upper bounds and the minimized function, even when the problem is nonconvex. In practice, the ε-constraint method may be less efficient to solve than the weighted sum method computationally, because the number of constraints increases. It may also be difficult to specify appropriate upper bounds for the objective functions.

3. Method of the Global Criterion

In this method, the distance between some reference point and the feasible objective region is minimized. Here, we apply the method where the utopian objective vector $z^* \in R^N$ is used as a reference point and l_p-metrics are used for distance measuring. The weighted l_p-problem is given by

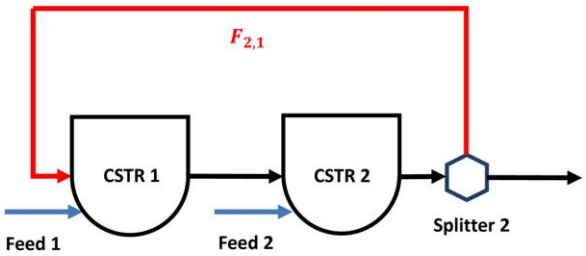

Figure 4. Superstructure of polymerization process (2 CSTRs).

[Color figure can be viewed in the online issue, which is available at wileyonlinelibrary.com.]

$$\min \left(\sum_{k=1}^{Q} w_k |f_k(x) - z_k^*|^p \right)^{1/p} \quad \text{s.t. } x \in S \tag{38}$$

where the components z_k^* of the utopian objective vector z^* are obtained by minimizing each of the objective functions individually. The optimal solution depends heavily on the value of p. Problem (38) becomes more poorly conditioned and more difficult to solve as the value increases. The solution of l_p-problem ($1 \le p < \infty$) is guaranteed to be Pareto optimal. However, not necessarily all of the Pareto optimal solutions could be identified, which depends on the degree of nonconvexity of the problem.

MO problem formulations

Modified Weighted Sum Formulation. To select the MO method we consider the designed MWD profile for the polymer product quality requirement. Our aim is to maximize monomer conversion and minimize the deviation between the calculated and target MWDs. MWD can be considered to be a vector of sampling points on the MWD curve. The deviation between the kth sampling points on the calculated and target MWDs can be expressed as $|\mathrm{MWD}^k_{\mathrm{calc}} - \mathrm{MWD}^k_{\mathrm{tar}}|$, where $\mathrm{MWD}^k_{\mathrm{calc}}$ and $\mathrm{MWD}^k_{\mathrm{tar}}$ are the values of the kth sampling points on the calculated and target MWDs, respectively. The ε-constraint method is a rather natural and intuitive choice to solve the MO problem. It comprises an NLP problem with a monomer conversion objective function, constraint functions imposed by the product quality requirement and the superstructure process model equations

$$\begin{aligned} &\max_z \ \mathrm{MC} \\ &\text{s.t. } G_N(\mathrm{MWD}_{\mathrm{calc}}, z) = 0 \\ &z_{\mathrm{lb}} \le z \le z_{\mathrm{ub}} \\ &|\mathrm{MWD}^k_{\mathrm{calc}} - \mathrm{MWD}^k_{\mathrm{tar}}| \le \varepsilon_k, \ \ k = 1, \ldots, N_P \end{aligned} \tag{39}$$

where z is the vector of continuous decision variables, including split fractions and operating conditions (temperature, pressure, and liquid volume of the CSTR; feed flow rates of catalyst, hydrogen, ethylene, and hexane into the CSTR). z_{lb} and z_{ub} are the lower and upper bounds of decision variables based on the limitations of the equipment or chemical reaction technology. A positive lower bound on the CSTR liquid volume is imposed, ensuring the existence of the reactor. MC stands for monomer conversion. The equality constraint G_N relating $\mathrm{MWD}_{\mathrm{calc}}$ to z is the superstructure process model of N CSTRs, including the CSTR model and the connectivity equations (Eqs. 1–35). N_P is the number of sampling points comprising the MWD curve, set to 100 by our experience. ε_k is the kth MWD deviation tolerance. However, there is no a priori information to set the values of ε_k to obtain a desirable solution. Therefore, we embed the concept of weighted sum method into NLP (39) and form the following MO formulation

$$\begin{aligned} &\min_z \left(\sum_{k=1}^{N_P} w_k * \varepsilon_k \right) - w_0 * \mathrm{MC} \\ &\text{s.t. } G_N(\mathrm{MWD}_{\mathrm{calc}}, z) = 0 \\ &z_{\mathrm{lb}} \le z \le z_{\mathrm{ub}} \\ &|\mathrm{MWD}^k_{\mathrm{calc}} - \mathrm{MWD}^k_{\mathrm{tar}}| \le \varepsilon_k, \ \ k = 1, \ldots, N_P \end{aligned} \tag{40}$$

where the MWD deviation tolerances appear in the objective function and are multiplied by the weighting factors. This problem can be regarded as a *modified weighted sum formulation*

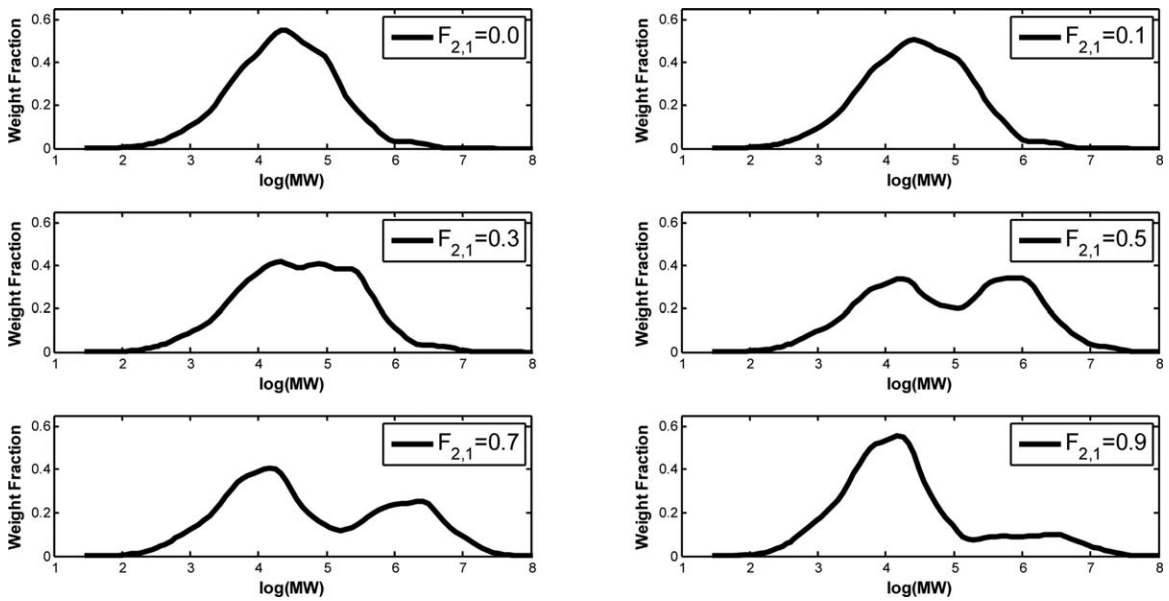

Figure 5. MWD simulation results under different values of split fraction $F_{2,1}$.

with the extra MWD specification constraints. Instead of setting ε_k to fixed values, NLP (40) has more degrees of freedom, allowing us to analyze and choose the tolerance values more freely. There are systematic ways[38] of altering the weighting factors to generate different Pareto solutions. Very often an *ad hoc* numerical solution procedure is required to solve a number of problems with different sets of weighting factors.

Normalized Global Criterion Formulation. Based on the basic method of the global criterion in (38), denominators are added to normalize the components in the objective function. The *normalized global criterion formulation* is

$$\begin{aligned} &\min_z \ ([(\mathrm{MC}^*-\mathrm{MC})/\mathrm{MC}^*]^p+[(\varepsilon-\varepsilon^*)/\varepsilon^*]^p)^{1/p} \\ &\text{s.t. } G_N(\mathrm{MWD}_{\mathrm{calc}}, z)=0 \\ &z_{\mathrm{lb}} \le z \le z_{\mathrm{ub}} \\ &|\mathrm{MWD}^k_{\mathrm{calc}}-\mathrm{MWD}^k_{\mathrm{tar}}| \le \varepsilon, \ \ k=1, \ldots, N_P \end{aligned} \tag{41}$$

where MC^* and ε^* stand for the utopian monomer conversion and MWD deviation tolerance, respectively. Utopian values MC^* and ε^* can be obtained by maximizing MC and minimizing ε individually, as shown in NLPs (42) and (43), respectively

$$\begin{aligned} &\min_z \ -\mathrm{MC} \\ &\text{s.t. } G_N(z)=0 \\ &z_{\mathrm{lb}} \le z \le z_{\mathrm{ub}} \end{aligned} \tag{42}$$

$$\begin{aligned} &\min_z \ \varepsilon \\ &\text{s.t. } G_N(\mathrm{MWD}_{\mathrm{calc}}, z)=0 \\ &z_{\mathrm{lb}} \le z \le z_{\mathrm{ub}} \\ &|\mathrm{MWD}^k_{\mathrm{calc}}-\mathrm{MWD}^k_{\mathrm{tar}}| \le \varepsilon, \ \ k=1, \ldots, N_P \end{aligned} \tag{43}$$

Note that the denominators in (41) compensate for the corresponding variable scales and provide a relative distance minimization from the utopia point. The inequality constraints of MWD deviations are also included here. Compared to NLP (40), there are only three problems to be solved with considerably less computational effort. The solution with the l_p-metrics ($1 \le p < \infty$) is guaranteed to be Pareto optimal. In the following case studies, we consider and compare solutions with NLPs (40) and (41).

Results and Discussion

In this study, AMPL, an EO optimization modeling system, was used to construct the complete problem formulation. The problems were numerically solved using IPOPT 3.10 on Dell Inspiron N4110 running 64-bit Windows 7 with a 2.30 GHz Intel Core i5 processor and 6 GB RAM. In IPOPT, uniqueness of the (locally) optimal solution has been confirmed through nonsingularity of the KKT matrix and satisfaction of sufficient second order conditions at the solution. Therefore, the solution is at least locally unique and isolated. This is an important property inherent in IPOPT, as described in Zavala et al.[39] Conversely, no guarantee can be given that the solution is globally optimal, mainly due to the nonconvexity of the problem. However, in our work, the initial values of decision variables were set to a hundred different datasets for multistart optimizations. This systematic multistart initialization procedure could be considered as a practical alternative to global optimization. From these starting points, we converged to the same optimal solution every time. This lends confidence that these results cannot be improved further.

Impact of reactor network on MWD

Several simulation cases based on the superstructure model are first presented to reflect the impact of this reactor network on MWD. From the numerical results below, the process superstructure shows its potential capability and flexibility. We consider the polymerization process superstructure of two CSTRs with one splitter as a special scenario, as shown in Figure 4. Through Splitter 2, fraction $F_{2,1}$ of the polymer stream leaving CSTR 2 is fed back into CSTR 1 while the remaining one flows into downstream process units. The split fraction $F_{2,1}$ can vary in the range [0, 1). Based on this flowsheet configuration, the simulation results of MWDs under different values of $F_{2,1}$ are illustrated in Figure 5. If $F_{2,1}$ is set to 0.0, we get a unimodal MWD with a serial configuration. When $F_{2,1}$ is 0.3, the distribution is trimodal, where three visible molecular weight peaks appear on the MWD curve. If $F_{2,1}$ is 0.5 or 0.7, the MWD becomes bimodal. When $F_{2,1}$ increases to 0.9, a typical unimodal MWD with a long tail is obtained. Hence, we can see that without major changes in the reactor network structure, different shapes of MWD can be obtained, thus leading to the improvement of the end-use properties and the development of new polymer grades.

Optimization with bimodal MWD

The bimodal MWD profile of polymers has two distinct molecular weight peaks. The low molecular weight peak provides good processability and the high molecular weight peak gives excellent mechanical strength, which is the advantage of bimodal polymers over conventional unimodals. In this scenario, we use a bimodal MWD as the target product quality and apply the two formulations (40) and (41) to solve the MO problem. This target MWD was generated from a simulation run with 4 CSTRs in series under a different range of operating conditions.

Modified Weighted Sum Formulation. We first consider cases with NLP (40). Here, the problem formulation is simplified to the following formulation with a uniform tolerance ε and a single weighting factor w. The number of CSTRs in the superstructure model varies from 1 to 4

$$\begin{aligned} &\min_z \ w*\varepsilon-\mathrm{MC} \\ &\text{s.t. } G_N(\mathrm{MWD}_{\mathrm{calc}}, z)=0 \\ &z_{\mathrm{lb}} \le z \le z_{\mathrm{ub}} \\ &|\mathrm{MWD}^k_{\mathrm{calc}}-\mathrm{MWD}^k_{\mathrm{tar}}| \le \varepsilon, \ \ k=1, \ldots, N_P \end{aligned} \tag{44}$$

Table 2. Average Iterations and CPU Time of IPOPT (Bimodal MWD)

Cases	Formulations	No. of Iterations	CPU Time (s)
1 CSTR	*Modified Weighted Sum*	136	8.7
	Normalized Global Criterion	170	11.0
2 CSTRs	*Modified Weighted Sum*	98	13.6
	Normalized Global Criterion	137	19.9
3 CSTRs	*Modified Weighted Sum*	179	44.5
	Normalized Global Criterion	204	49.9
4 CSTRs	*Modified Weighted Sum*	218	103.2
	Normalized Global Criterion	168	83.3

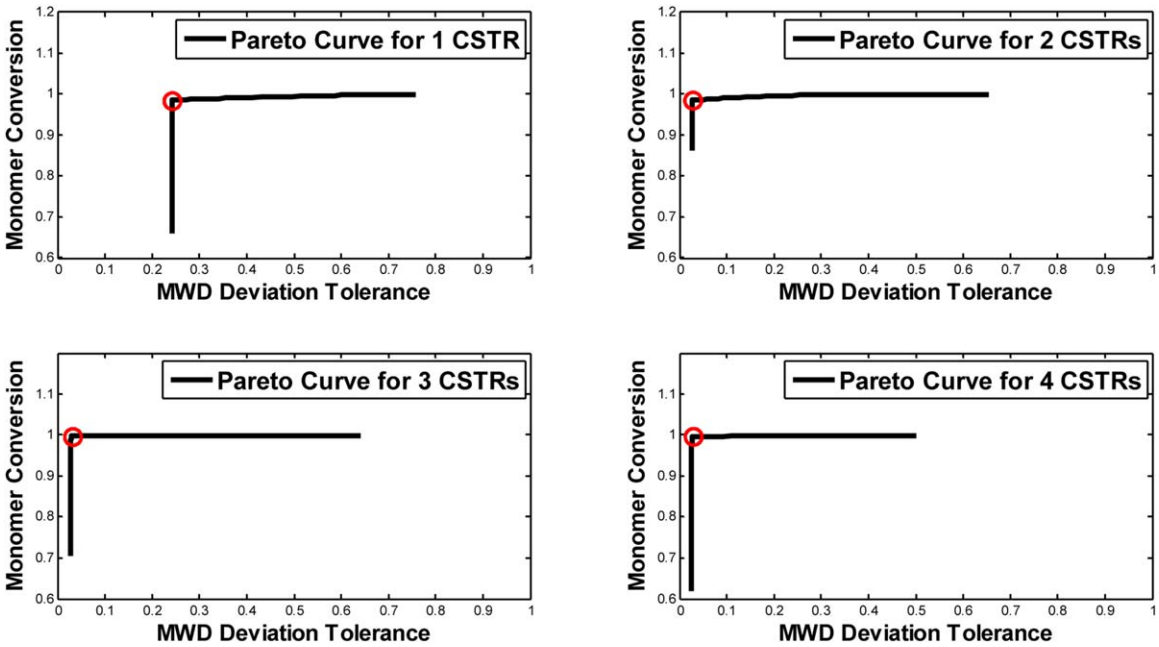

Figure 6. Pareto curves with different no. of CSTRs by *modified weighted sum formulation* (bimodal MWD).

[Color figure can be viewed in the online issue, which is available at wileyonlinelibrary.com.]

By altering the weighting factor w, different Pareto optimal solutions can be generated. It is clearly not practical to generate the entire set of Pareto solutions. The most one can expect is a representative subset from which a reasonably good, if not the best, trade-off of objectives can be selected.[38] In this scenario, the sequence of ten w's values were set to 0.01, 0.1, 1, …, 10,000,000 as a geometric series. Then, we solved a series of problems with the ten values of w and obtained a set of Pareto optimal solution points (ε, MC). The average numbers of iterations and CPU time IPOPT required for solving the problems with different numbers of CSTRs are listed in Table 2. The Pareto curves are formed based on these points, as shown in Figure 6. The x axis is MWD deviation tolerance ε and y axis is monomer conversion MC. For one CSTR, the Pareto curve appears as two very stiff line segments. On the vertical segment, with the decrease of w, ε is nearly unchanged while MC increases to a very high value. On the horizontal segment, with the decrease of w, MC becomes nearly unchanged while ε increases to a very high value. Naturally, we choose the turning point (with $w=1$) as our compromise solution. Similar results occur on the curves for 2, 3, and 4 CSTRs. The numerical results of the compromise solutions are listed in Table 3. All the values of MC are very close to 1, meaning that high conversion could be achieved. The corresponding optimized MWDs are illustrated in Figure 7. The solid black lines represent the target bimodal MWDs and the dotted red lines are the optimized MWDs. If only one CSTR is utilized, there is a huge difference between the optimized and target MWD curves, indicating that we are unable to meet this bimodal MWD requirement with only one CSTR. When two or more CSTRs are used, the MWD deviation becomes very small and acceptable. The same conclusion can be drawn from the values of ε in Table 3. The information on the corresponding optimal operating conditions for the cases with 1, 2, 3, and 4 CSTRs is given in Table 4, where T represents temperature, P represents pressure, V represents liquid volume, and FR represents flow rate. The information on the corresponding optimal split fractions for the cases with 2, 3, and 4 CSTRs is given in Table 5.

Normalized Global Criterion Formulation. We now apply the *normalized global criterion formulation* (41). Considering that the problem becomes more poorly conditioned and more difficult to solve as the value of p increases, the NLP (41) is simplified to the following NLP with $p=1$.

Table 3. Numerical Results of Optimal Solutions (Bimodal MWD)

Cases	Solutions	MC	ε	U
1 CSTR	Utopia	0.999077	0.241617	
	Modified Weighted Sum (w=1)	0.985991	0.241910	76.022
	Normalized Global Criterion	0.985991	0.241910	76.022
2 CSTRs	Utopia	0.999998	0.027673	
	Modified Weighted Sum (w=0.1)	0.985649	0.027685	**69.659**
	Normalized Global Criterion	0.985648	0.027685	69.654
3 CSTRs	Utopia	1.000000	0.027633	
	Modified Weighted Sum (w=10)	0.986549	0.027640	**74.331**
	Normalized Global Criterion	0.986546	0.027640	74.314
4 CSTRs	Utopia	1.000000	0.025359	
	Modified Weighted Sum (w=100)	0.965068	0.025717	26.542
	Normalized Global Criterion	0.968211	0.025765	**28.095**

The bold characters mean that the corresponding values are the final optimal solutions after comparison.

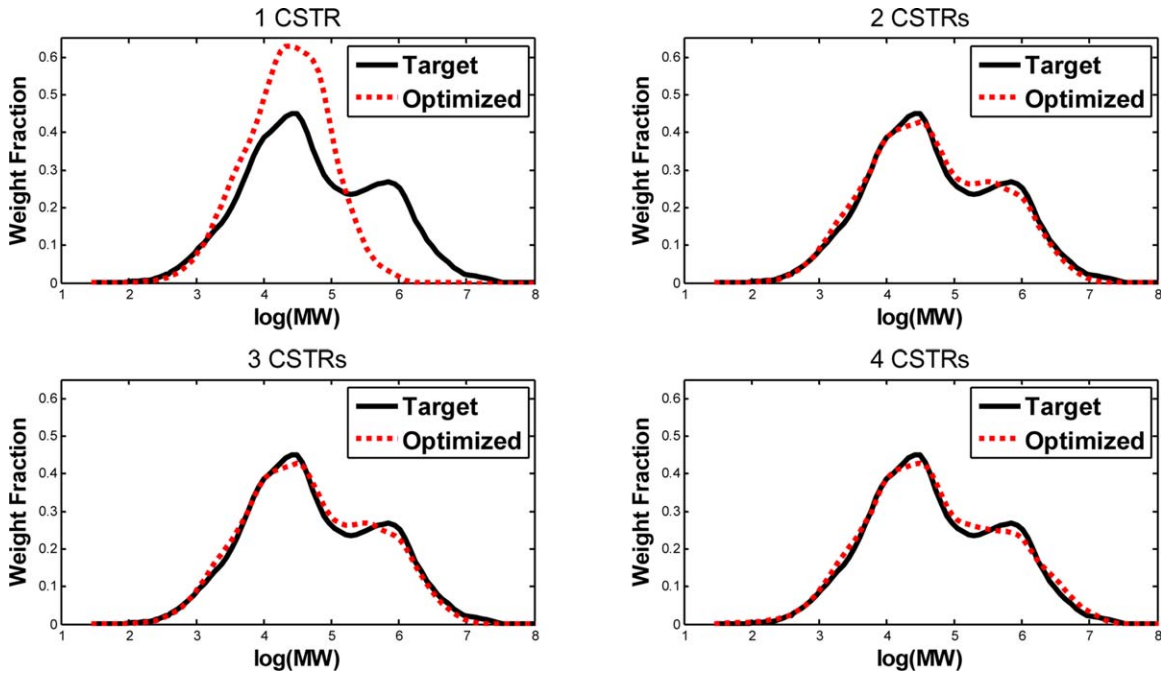

Figure 7. MWD optimization results with different no. of CSTRs by *modified weighted sum formulation* (bimodal MWD).

[Color figure can be viewed in the online issue, which is available at wileyonlinelibrary.com.]

$$\begin{aligned} &\min_{z} \ [(\mathrm{MC}^{*}-\mathrm{MC})/\mathrm{MC}^{*}]+[(\varepsilon-\varepsilon^{*})/\varepsilon^{*}] \\ &\text{s.t. } G_N(\mathrm{MWD}_{\mathrm{calc}}, z)=0 \\ &z_{\mathrm{lb}} \le z \le z_{\mathrm{ub}} \\ &|\mathrm{MWD}^{k}_{\mathrm{calc}}-\mathrm{MWD}^{k}_{\mathrm{tar}}| \le \varepsilon, \ \ k=1, \ldots, N_P \end{aligned} \tag{45}$$

First, we solved NLPs (42) and (43) to obtain the utopian values (ε^{*}, MC^{*}). Then, NLP (45) was solved using these two utopian values in the objective function. The average numbers of iterations and CPU time IPOPT required for solving the problems with different numbers of CSTRs are listed in Table 2. Although there is not much difference

Table 4. Data of Optimal Operating Conditions by *Modified Weighted Sum Formulation* (Bimodal MWD)

Subsystems	Conditions	CSTR1	CSTR2	CSTR3	CSTR4	Lower Bounds	Upper Bounds
Catalyst	FR (kmol/h)	0. 40				10^{-8}	∞
Ethylene	FR (kmol/h)	79.21				10^{-8}	∞
Hydrogen	FR (kmol/h)	0.31				10^{-8}	∞
Hexane	FR (kmol/h)	0.12				10^{-8}	∞
Reactor	T (K)	358.15*				340.15	358.15
	P (kPa)	354.64*				354.64	759.94
	V (m^3)	34.93				10^{-3}	35.00
Catalyst	FR (kmol/h)	0.96	1.63×10^{-6}			10^{-8}	∞
Ethylene	FR (kmol/h)	122.10	76.86			10^{-8}	∞
Hydrogen	FR (kmol/h)	0.80	6.62×10^{-8}			10^{-8}	∞
Hexane	FR (kmol/h)	29.71	1.45×10^{-5}			10^{-8}	∞
Reactor	T (K)	355.38	358.15*			340.15	358.15
	P (kPa)	368.79	354.64*			354.64	759.94
	V (m^3)	35.00*	35.00*			10^{-3}	35.00
Catalyst	FR (kmol/h)	0.88	0.077	0.42		10^{-8}	∞
Ethylene	FR (kmol/h)	97.31	73.90	81.27		10^{-8}	∞
Hydrogen	FR (kmol/h)	2.74×10^{-5}	0.53	0.50		10^{-8}	∞
Hexane	FR (kmol/h)	11.73	0.0071	0.0064		10^{-8}	∞
Reactor	T (K)	358.15*	343.38	358.15*		340.15	358.15
	P (kPa)	354.64*	385.55	354.64*		354.64	759.94
	V (m^3)	24.95	35.00*	35.00*		10^{-3}	35.00
Catalyst	FR (kmol/h)	0.28	2.77×10^{-7}	1.51×10^{-7}	1.39×10^{-7}	10^{-8}	∞
Ethylene	FR (kmol/h)	49.16	21.26	10.64	4.16×10^{-7}	10^{-8}	∞
Hydrogen	FR (kmol/h)	0.32	9.86×10^{-5}	6.57×10^{-4}	48.83	10^{-8}	∞
Hexane	FR (kmol/h)	1.51×10^{-6}	1.52×10^{-6}	1.53×10^{-6}	1.66×10^{-6}	10^{-8}	∞
Reactor	T (K)	358.15*	358.15*	358.15*	351.50	340.15	358.15
	P (kPa)	354.64*	354.64*	354.64*	354.64*	354.64	759.94
	V (m^3)	35.00*	33.41	35.00*	35.00*	10^{-3}	35.00

*Represents an active bound.

Table 5. Data of Optimal Split Fractions by *Modified Weighted Sum Formulation* (Bimodal MWD)

Cases		To CSTR 1	To CSTR 2	To CSTR 3	To CSTR 4	Downstream
2 CSTRs	From CSTR 1	–	1 (fixed)			
	From CSTR 2	0.213	–			0.787
3 CSTRs	From CSTR 1	–	1	0		
	From CSTR 2	0.326	–	0.674		
	From CSTR 3	0	0	–		1
4 CSTRs	From CSTR 1	–	0.485	0	0.515	
	From CSTR 2	0.457	–	0.543	0	
	From CSTR 3	0	0.052	–	0.948	
	From CSTR 4	0	0	0	–	1

between the average numbers of iterations and CPU time of the two formulations, the *normalized global criterion formulation* requires solution of only one problem (45) instead of solving several problems with the *modified weighted sum formulation*. The numerical results of the optimal solutions are listed in Table 3. All the values of MC are very close to 1, meaning that high conversion could be achieved. The corresponding optimized MWDs are illustrated in Figure 8. A similar conclusion, that the MWD deviation becomes acceptable when two or more CSTRs are used, can be drawn from Figure 8 and the values of ε in Table 3. The information on the corresponding optimal operating conditions for the cases with 1, 2, 3, and 4 CSTRs is given in Table 6. The information on the corresponding optimal split fractions for the cases with 2, 3, and 4 CSTRs is given in Table 7. A threshold, 10^{-8} in our cases, is used to round-off the split fraction. If it is less than the threshold, we regard it as a zero.

Comparison of MO formulations

In Table 3, the optimal solutions of the *modified weighted sum formulation* and *normalized global criterion formulation* are very similar to each other. As the decision maker, we could specify our further preferences between the results of the two formulations.[37] We compare these results by choosing the following underlying value function, given by $U: R^2 \rightarrow R$

$$U(\varepsilon, \mathrm{MC}) = 1/\left([(\varepsilon - \varepsilon^*)/\varepsilon^*]^2 + [(\mathrm{MC}^* - \mathrm{MC})/\mathrm{MC}^*]^2 \right)^{1/2} \quad (46)$$

which is the reciprocal of the Euclidean distance (2-norm distance) between the utopia point (ε^*, MC^*) and the optimal solution (ε, MC). Our expectation is that the optimal solution should be as close as possible to the utopia point in geometry. According to the expression (46), we can rank the optimal solutions with different numbers of CSTRs and select the final solutions whose values of U are higher. The last column of Table 3 shows the numerical results of the value function. In the case of 1 CSTR, the solutions of the two formulations are equally desirable. In the cases of 2 and 3 CSTRs, the solutions of the *modified weighted sum formulation* are chosen. In the case of 4 CSTRs, we prefer the solution of the *normalized global criterion formulation*. After the selection, the final optimal flowsheet configurations of 2, 3, 4 CSTRs are illustrated in Figures 9, 10 and 11. These optimal structural designs are easy to achieve in practice.

Optimization with trimodal MWD

Trimodal polyolefins are regarded as the next key advance in polymer products. In this scenario, we use a trimodal MWD

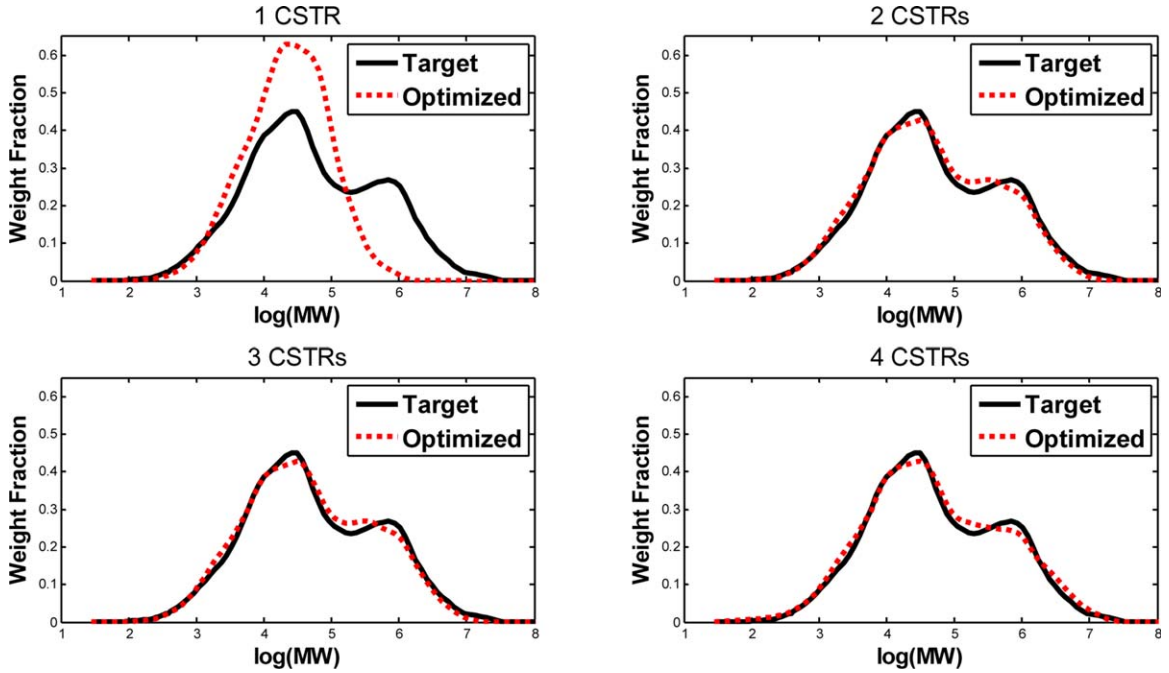

Figure 8. MWD optimization results with different no. of CSTRs by *normalized global criterion formulation* (bimodal MWD).

[Color figure can be viewed in the online issue, which is available at wileyonlinelibrary.com.]

Table 6. Data of Optimal Operating Conditions by *Normalized Global Criterion Formulation* (Bimodal MWD)

Subsystems	Conditions	CSTR1	CSTR2	CSTR3	CSTR4	Lower Bounds	Upper Bounds
Catalyst	FR (kmol/h)	0.40				10^{-8}	∞
Ethylene	FR (kmol/h)	79.04				10^{-8}	∞
Hydrogen	FR (kmol/h)	0.31				10^{-8}	∞
Hexane	FR (kmol/h)	3.54×10^{-5}				10^{-8}	∞
Reactor	T (K)	358.15*				340.15	358.15
	P (kPa)	354.64*				354.64	759.94
	V (m^3)	35.00*				10^{-3}	35.00
Catalyst	FR (kmol/h)	0.96	2.76×10^{-6}			10^{-8}	∞
Ethylene	FR (kmol/h)	122.10	76.86			10^{-8}	∞
Hydrogen	FR (kmol/h)	0.80	5.71×10^{-8}			10^{-8}	∞
Hexane	FR (kmol/h)	29.71	2.98×10^{-5}			10^{-8}	∞
Reactor	T (K)	355.38	358.15*			340.15	358.15
	P (kPa)	368.79	354.64*			354.64	759.94
	V (m^3)	35.00*	35.00*			10^{-3}	35.00
Catalyst	FR (kmol/h)	0.88	0.078	0.41		10^{-8}	∞
Ethylene	FR (kmol/h)	97.35	74.20	81.03		10^{-8}	∞
Hydrogen	FR (kmol/h)	2.93×10^{-7}	0.54	0.50		10^{-8}	∞
Hexane	FR (kmol/h)	11.83	8.19×10^{-5}	7.71×10^{-5}		10^{-8}	∞
Reactor	T (K)	358.15*	343.40	358.15*		340.15	358.15
	P (kPa)	354.64*	386.15	354.64*		354.64	759.94
	V (m^3)	24.91	35.00*	35.00*		10^{-3}	35.00
Catalyst	FR (kmol/h)	1.10×10^{-7}	9.13×10^{-8}	0.36	2.19×10^{-7}	10^{-8}	∞
Ethylene	FR (kmol/h)	20.92	10.82	49.17	1.52×10^{-7}	10^{-8}	∞
Hydrogen	FR (kmol/h)	2.20×10^{-8}	3.93×10^{-4}	0.32	49.14	10^{-8}	∞
Hexane	FR (kmol/h)	6.53×10^{-7}	6.54×10^{-7}	6.69×10^{-7}	7.53×10^{-7}	10^{-8}	∞
Reactor	T (K)	358.15*	358.15*	358.15*	350.55	340.15	358.15
	P (kPa)	355.92	354.64*	354.64*	354.64*	354.64	759.94
	V (m^3)	35.00*	27.06	35.00*	35.00*	10^{-3}	35.00

*Represents an active bound.

Table 7. Data of Optimal Split Fractions by *Normalized Global Criterion Formulation* (Bimodal MWD)

Cases		To CSTR 1	To CSTR 2	To CSTR 3	To CSTR 4	Downstream
2 CSTRs	From CSTR 1	–	1 (fixed)			
	From CSTR 2	0.213	–			0.787
3 CSTRs	From CSTR 1	–	1	0		
	From CSTR 2	0.325	–	0.675		
	From CSTR 3	0	0	–		1
4 CSTRs	From CSTR 1	–	1	0	0	
	From CSTR 2	0.039	–	0.583	0.378	
	From CSTR 3	0.322	0.016	–	0.662	
	From CSTR 4	0	0	0	–	1

as the target product quality and apply the two formulations (44) and (45) to solve the MO problem. This target MWD was also generated from a simulation run with 4 CSTRs in series under a different range of operating conditions. Here, the aim is to explore the potential capability and flexibility of the process superstructure. The main issue is whether the trimodal polymer could be produced with less than 4 CSTRs. Hence, the number of CSTRs in the superstructure model varies from 1 to 3. However, according to our numerical results, the process superstructures (1 and 2 CSTRs) fail to achieve an acceptable MWD deviation. Thus, the case study below uses the superstructure of 3 CSTRs only.

We first apply the *modified weighted sum formulation* (44). Similarly, a series of problems with the aforementioned ten values of w are solved and a set of Pareto optimal solution points (ε, MC) are obtained. The Pareto curve is formed based on these points, as shown in Figure 12. Naturally, we choose the turning point (with $w=1000$) as our compromise solution. The average number of iterations is 201 and CPU time is

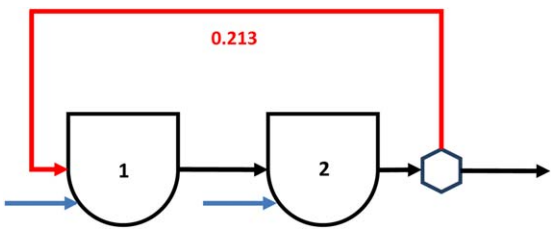

Figure 9. Optimal flowsheet configuration of polymerization process with 2 CSTRs (bimodal MWD).

[Color figure can be viewed in the online issue, which is available at wileyonlinelibrary.com.]

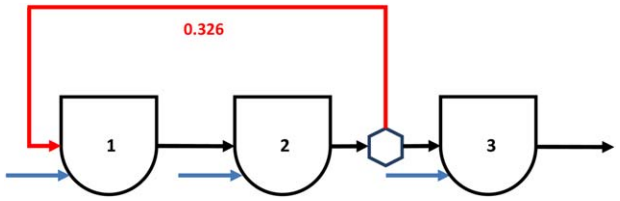

Figure 10. Optimal flowsheet configuration of polymerization process with 3 CSTRs (bimodal MWD).

[Color figure can be viewed in the online issue, which is available at wileyonlinelibrary.com.]

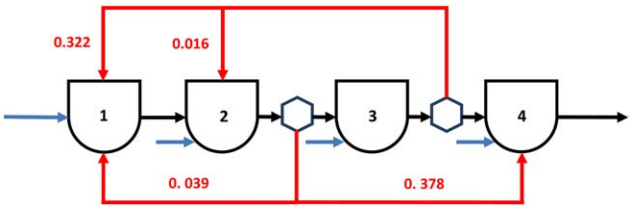

Figure 11. Optimal flowsheet configuration of polymerization process with 4 CSTRs (bimodal MWD).

[Color figure can be viewed in the online issue, which is available at wileyonlinelibrary.com.]

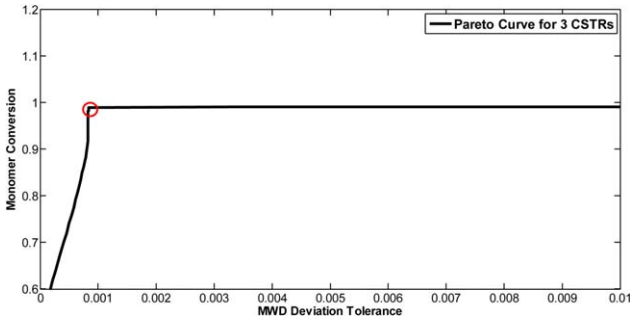

Figure 12. Pareto curve with 3 CSTRs by *modified weighted sum formulation* (trimodal MWD).

[Color figure can be viewed in the online issue, which is available at wileyonlinelibrary.com.]

63.3 s. For the *normalized global criterion formulation* (45), the average number of iterations is 220 and CPU time is 72.1 s. The numerical results of the optimal solutions by the two formulations are listed in Table 8. Both the values of MC are very close to 1, meaning that high conversion could be achieved. The small values of ε indicate that we are able to meet this trimodal MWD requirement with a 3 CSTR network. The corresponding optimized MWDs are illustrated in Figure 13. The optimized curves achieve excellent agreement with the target curves. The information on the corresponding

Table 8. Numerical Results of Optimal Solutions (Trimodal MWD)

Case	Solutions	*MC*	ε	*U*
3 CSTRs	Utopia	1.000000	0.000126	
	Modified Weighted Sum (w=1000)	0.987159	0.000834	0.177
	Normalized Global Criterion	0.973821	0.000828	**0.179**

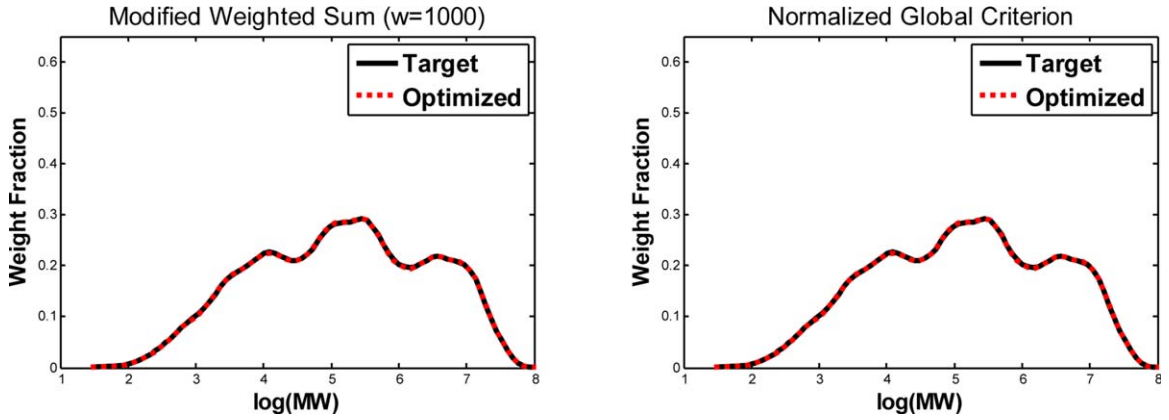

Figure 13. MWD optimization results with 3 CSTRs by two formulations (trimodal MWD).

[Color figure can be viewed in the online issue, which is available at wileyonlinelibrary.com.]

Table 9. Data of Optimal Operating Conditions by Two Formulations (Trimodal MWD)

Formulations	Subsystems	Conditions	CSTR1	CSTR2	CSTR3	Lower Bounds	Upper Bounds
Modified Weighted Sum (w=1000)	Catalyst	FR (kmol/h)	0.14	0.29	0.36	10^{-8}	∞
	Ethylene	FR (kmol/h)	74.53	53.58	36.96	10^{-8}	∞
	Hydrogen	FR (kmol/h)	0.04	9.10×10^{-4}	1.07	10^{-8}	∞
	Hexane	FR (kmol/h)	1.02×10^{-6}	1.02×10^{-6}	1.02×10^{-6}	10^{-8}	∞
	Reactor	*T* (K)	340.15*	358.15*	358.15*	340.15	358.15
		P (kPa)	759.94*	549.32	354.64*	354.64	759.94
		V (m^3)	27.60	10.89	35.00*	10^{-3}	35.00
Normalized Global Criterion	Catalyst	FR (kmol/h)	0.10	0.13	0.09	10^{-8}	∞
	Ethylene	FR (kmol/h)	41.32	26.91	13.78	10^{-8}	∞
	Hydrogen	FR (kmol/h)	1.10×10^{-8}	6.26×10^{-5}	0.61	10^{-8}	∞
	Hexane	FR (kmol/h)	1.99×10^{-7}	1.98×10^{-7}	1.98×10^{-7}	10^{-8}	∞
	Reactor	*T* (K)	340.15*	358.15*	358.15*	340.15	358.15
		P (kPa)	759.94*	506.90	354.64*	354.64	759.94
		V (m^3)	17.13	10.56	35.00*	10^{-3}	35.00

*Represents an active bound.

Table 10. Data of Optimal Split Fractions by Two Formulations (Trimodal MWD)

Formulations		To CSTR 1	To CSTR 2	To CSTR 3	Downstream
Modified Weighted Sum (w=1000)	From CSTR 1	–	0.056	0.944	
	From CSTR 2	0	–	1	
	From CSTR 3	0.137	0	–	0.863
Normalized Global Criterion	From CSTR 1	–	0.083	0.917	
	From CSTR 2	0	–	1	
	From CSTR 3	0.216	0	–	0.784

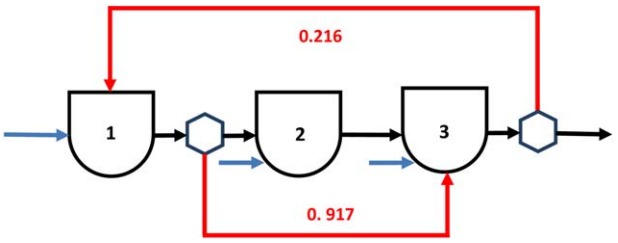

Figure 14. Optimal flowsheet configuration of polymerization process with 3 CSTRs (trimodal MWD).

[Color figure can be viewed in the online issue, which is available at wileyonlinelibrary.com.]

optimal operating conditions for the case is given in Table 9. The information on the corresponding optimal split fractions for the case is given in Table 10. Using the value function (46), we choose the solution of the *normalized global criterion formulation* as our final optimal solution. The final optimal flowsheet configuration with 3 CSTRs is illustrated in Figure 14. As seen from the numerical results, it is enough to use 3 CSTRs with splitters to produce the trimodal HDPE product with the desired MWD and high monomer conversion.

Conclusions

A systematic reactor network synthesis approach is proposed to generate optimal flowsheet configurations of polymerization processes. On the basis of an industrial HDPE slurry process model with embedded MWD calculation, a generalized polymerization process superstructure of CSTRs is established through the introduction of splitters. By applying a variety of MO methods, the two NLP formulations of *modified weighted sum* and *normalized global criterion* are developed to simultaneously maximize the monomer conversion and to minimize the deviation between the calculated and target MWDs. The optimal reactor network structure and operating policies are obtained by systematically manipulating a set of continuous decision variables.

The effectiveness and efficiency of the proposed synthesis approach are illustrated with several case studies that consider different specifications on MWD, including a bimodal profile and a trimodal profile. A simulation case study is first presented to reflect the impact of this reactor network superstructure on the development of different MWDs. Then, after solving two types of MO problems, the numerical solutions are compared and the final decisions are made based on an underlying value function. Numerical results show that the optimal flowsheet configurations overcome the limitations of conventional reactor network structures and help to increase reactor productivity at the desired product quality in polymerization processes. We believe that this approach can be generalized to other chemical systems where the reactor network structure can be exploited by introducing additional process units and their potential interconnections. Thus, more general superstructure models could be established and applied to enhance the performance of reactor networks.

Acknowledgments

We gratefully acknowledge the financial support of 973 Program of China (No. 2012CB720503) and National Natural Science Foundation of China (No. 61374205).

Literature Cited

1. Asteasuain M, Bandoni A, Sarmoria C, Brandolin A. Simultaneous process and control system design for grade transition in styrene polymerization. *Chem Eng Sci*. 2006;61:3362–3378.
2. Chen X, Chen L, Feng J, Yao Z, Qian JX. Toward polymer product design. I. Dynamic optimization of average molecular weights and polydispersity index in batch free radical polymerization. *Ind Eng Chem Res*. 2009;48:6739–6748.
3. Achenie LKE, Biegler LT. Algorithmic synthesis of chemical reactor networks using mathematical-programming. *Ind Eng Chem Fund*. 1986;25:621–627.
4. Achenie LKE, Biegler LT. A superstructure based approach to chemical reactor network synthesis. *Comput Chem Eng*. 1990;14:23–40.
5. Kokossis AC, Floudas CA. Synthesis of isothermal reactor separator recycle systems. *Chem Eng Sci*. 1991;46:1361–1683.
6. Kokossis AC, Floudas CA. Optimization of complex reactor networks. 2. Nonisothermal operation. *Chem Eng Sci*. 1994;49:1037–1051.
7. Peschel A, Freund H, Sundmacher K. Methodology for the design of optimal chemical reactors based on the concept of elementary process functions. *Ind Eng Chem Res*. 2010;49:10535–10548.
8. Soares JBP. Mathematical modelling of the microstructure of polyolefins made by coordination polymerization: a review. *Chem Eng Sci*. 2001;56:4131–4153.
9. Crowley TJ, Choi KY. Control of molecular weight distribution and tensile strength in a free radical styrene polymerization process. *J Appl Polym Sci*. 1998;70:1017–1026.
10. Wells GJ, Ray WH. Prediction of polymer properties in LDPE reactors. *Macromol Mater Eng*. 2005;290:319–346.
11. Ali MA, Ajbar EAA, Alhumaizi K. Control of molecular weight distribution of polyethylene in gas-phase fluidized bed reactors. *Korean J Chem Eng*. 2010;27:364–372.
12. Ali MA, Ali EM. Effect of monomer feed and production rate on the control of molecular weight distribution of polyethylene in gas phase reactors. *Comput Chem Eng*. 2011;35:2480–2490.
13. Pontes KV, Embiruçu M, Maciel R, Hartwich A, Marquardt W. Optimal process operation for the production of linear polyethylene resins with tailored molecular weight distribution. *AIChE J*. 2011;57:2149–2163.
14. Weng JZ, Shao ZJ, Chen X, Gu XP, Yao Z, Feng LF, Biegler LT. A novel strategy for dynamic optimization of grade transition processes based on molecular weight distribution. *AIChE J*. 2014;60:2498–2512.
15. Flores-Tlacuahuac A, Rivera-Toledo M. A multiobjective dynamic optimization approach for a methyl-methacrylate plastic sheet reactor. *Macromol React Eng*. 2014;8:358–373.
16. Bhaskar V, Gupta SK, Ray AK. Multiobjective optimization of an industrial wiped film poly(ethylene terephthalate) reactor: some further insights. *Comput Chem Eng*. 2001;25:391–407.

17. Benyahia B, Latifi MA, Fonteix C, Pla F. Multicriteria dynamic optimization of an emulsion copolymerization reactor. *Comput Chem Eng*. 2011;35:2886–2895.
18. Massebeuf S, Fonteix C, Hoppe S, Pla F. Development of new concepts for the control of polymerization processes: multiobjective optimization and decision engineering. I. Application to emulsion homopolymerization of styrene. *J Appl Polym Sci*. 2003;87:2383–2396.
19. Costa EF, Lage PLC, Biscaia EC. On the numerical solution and optimization of styrene polymerization in tubular reactors. *Comput Chem Eng*. 2003;27:1591–1604.
20. Asteasuain M, Ugrin PE, Lacunza MH, Brandolin A. Effect of multiple feedings in the operation of a high-pressure polymerization reactor for ethylene polymerization. *Polym React Eng*. 2001;9:163–182.
21. Asteasuain M, Sarmoria C, Brandolin A, Bandoni A. Integration of control aspects and uncertainty in the process design of polymerization reactors. *Chem Eng J*. 2007;131:135–144.
22. Fontes CH, Mendes MJ. Analysis of an industrial continuous slurry reactor for ethylene-butene copolymerization. *Polymer*. 2005;46:2922–2932.
23. Gross J, Sadowski G. Perturbed-chain SAFT: an equation of state based on a perturbation theory for chain molecules. *Ind Eng Chem Res*. 2001;40:1244–1260.
24. Cressie N. The origins of kriging. *Math Geol*. 1990;22:239–252.
25. Zhang C, Zhan ZL, Shao ZJ, Zhao YH, Chen X, Gu XP, Yao Z, Feng LF, Biegler LT. Equation-oriented optimization on an industrial high-density polyethylene slurry process with target molecular weight distribution. *Ind Eng Chem Res*. 2013;52:7240–7251.
26. Zhang C, Shao ZJ, Chen X, Yao Z, Gu XP, Biegler LT. Kinetic parameter estimation of HDPE slurry process from molecular weight distribution: estimability analysis and multistep methodology. *AIChE J*. 2014;60:3442–3459.
27. Ray WH. On the mathematical modelling of polymerization reactors. *J Macromol Sci R M C*. 1972;8:1–56.
28. Dubé M, Soares JBP, Penlidis A, Hamielec AE. Mathematical modelling of multicomponent chain-growth polymerization in batch, semi-batch and continuous reactors. *Ind Eng Chem Res*. 1997;36:966–1015.
29. Flory PJ. *Principles of Polymer Chemistry*. New York: Cornell University Press, 1953.
30. Vickroy VV, Schneider H, Abbott RF. The separation of SEC curves of HDPE into Flory distributions. *J Appl Polym Sci*. 1993;50:551–554.
31. Soares JBP. A second look at modeling the multiplicity of active site types of Ziegler-Natta catalysts with Flory's and Stockmayer's distributions. *Polym React Eng*. 1998;6:225–241.
32. Hamielec AE, Tobita H. *Polymerization Processes*. Weinheim: Wiley-VCH Verlag GmbH & Co. KGaA, 2005.
33. Soares JBP, McKenna TFL. *Polyolefin Reaction Engineering*. Weinheim: Wiley-VCH Verlag GmbH & Co. KGaA, 2012.
34. Alghyamah AA, Soares JBP. Simultaneous deconvolution of the bivariate distribution of molecular weight and chemical composition of polyolefins made with Ziegler-Natta catalysts. *Macromol Rapid Commun*. 2009;30:384–393.
35. Khare NP, Seavey KC, Liu YA, Ramanathan S, Lingard S, Chen CC. Steady-state and dynamic modeling of commercial slurry high-density polyethylene (HDPE) processes. *Ind Eng Chem Res*. 2002;41:5601–5618.
36. Luyben ML, Floudas CA. Analyzing the interaction of design and control—1. A multiobjective framework and application to binary distillation synthesis. *Comput Chem Eng*. 1994;18:933–969.
37. Miettinen KM. *Nonlinear Multiobjective Optimization*. Boston: Kluwer Academic Publishers, 1999.
38. Chankong V, Haimes YY. *Multiobjective Decision Making: Theory and Methodology*. New York: North Holland, 1983.
39. Zavala VM, Laird CD, Biegler LT. Interior-point decomposition approaches for parallel solution of large-scale nonlinear parameter estimation problems. *Chem Eng Sci*. 2008;63:4834–4845.

Manuscript received May 22, 2015, and revision received Aug. 23, 2015.